NASA TECHNICAL NOTE

NASA TN D-4462

c. 1

NASA TN D-4462

PERFORMANCE OF ANNULAR PLUG AND EXPANSION-DEFLECTION NOZZLES INCLUDING EXTERNAL FLOW EFFECTS AT TRANSONIC MACH NUMBERS

by Robert A. Wasko

Lewis Research Center
Cleveland, Ohio

NATIONAL AERONAUTICS AND SPACE ADMINISTRATION • WASHINGTON, D. C. • APRIL 1968

ERRATA

NASA Technical Note D-4462

PERFORMANCE OF ANNULAR PLUG AND EXPANSION-DEFLECTION NOZZLES INCLUDING EXTERNAL FLOW EFFECTS AT TRANSONIC MACH NUMBERS

completed 17 Sep 69 - SW

By Robert A. Wasko

April 1968

Page 6, figure 4(a): The radius arrow at the widest point on the plug should be labeled R_2.

Page 6, figure 4(a) and page 8, figure 4(d): The dimensions for the second arrow from the left should be 5.5 (13.97).

Page 15, figure 7(b): In the ordinate scale the numbers .92 and .88 should be .93 and .89.

Page 18, figure 9(a): The ordinate scale for the two bottom plots should read 1.00, .98, .96.

Page 21, figure 9(d): The symbols for nozzle pressure ratio should be P_c/p_0.

Page 27, figure 15: The abscissa scale should read 60, 80, 100, 200, 300, 400, 600, 800.

Page 30: Line 15 should read "than that of the C-D nozzle, whereas the 0- and 10-percent plug nozzle per - "

NASA-Langley, 1968

Issued 7-30-68

NASA TN D-4462

PERFORMANCE OF ANNULAR PLUG AND EXPANSION-DEFLECTION NOZZLES INCLUDING EXTERNAL FLOW EFFECTS AT TRANSONIC MACH NUMBERS

By Robert A. Wasko

Lewis Research Center
Cleveland, Ohio

NATIONAL AERONAUTICS AND SPACE ADMINISTRATION

For sale by the Clearinghouse for Federal Scientific and Technical Information
Springfield, Virginia 22151 – CFSTI price $3.00

PERFORMANCE OF ANNULAR PLUG AND EXPANSION-DEFLECTION NOZZLES INCLUDING EXTERNAL FLOW EFFECTS AT TRANSONIC MACH NUMBERS

by Robert A. Wasko

Lewis Research Center

SUMMARY

An experimental investigation was made of the performance of annular plug and expansion-deflection (E-D) nozzles, and included the effects of external flow at Mach numbers from 0.56 to 2.0. The effects of base bleed were also studied, as well as geometry variations that included plug length and nozzle internal expansion. The full-length plug nozzle provided a nearly constant and optimum quiescent performance, whereas the E-D nozzle performance was only comparable with that of a conical convergent-divergent (C-D) nozzle. Thus, the plug nozzle was altitude compensating, whereas the E-D nozzle was not. The efficiency of the plug nozzle ranged from 98.4 percent at a pressure ratio of 68 (corresponding to sea-level altitude) to 99 percent at the design pressure ratio of 290. Efficiencies of the E-D and C-D nozzles were, respectively, 92.3 and 92.6 percent at sea level, and 97.6 and 97.8 percent at the design point. Truncation of the plug nozzles with internal expansion to a nominal 21, 10, and 0 percent of the full plug length resulted in decreased nozzle performance that varied from 96.4, 95.3, and 94.9 percent at sea level to 98.3, 97.0, and 96.8 percent, respectively, at the design point. Base bleed, in corrected amounts as small as 1.5 percent of the primary flow, produced improvements of the truncated plug nozzles with internal expansion, such that even the 0-percent-length plug nozzle (i.e., fully truncated) had a performance that was better than or comparable with that of a C-D nozzle. However, the E-D nozzle performance was improved only at pressure ratios above design. Elimination of both the internal expansion and the external plug surface resulted in poor nozzle performance, even with secondary flow. External flow effects were small and confined to a limited Mach number range. The maximum loss in performance was approximately 2.5 percent of the nozzle ideal thrust and occurred below Mach 1.0. Secondary flow reduced the performance loss to as little as 1.75 percent of ideal thrust.

INTRODUCTION

In recent years, various nozzle concepts have been proposed for advancing the technology of rocket propulsion systems. Application of this advancement to future boost vehicles may produce improvements in payload capability as well as reductions in mission costs. Particular emphasis has been placed on obtaining near optimum nozzle performance over a wide range of flight conditions since conventional convergent-divergent (C-D) nozzles, currently used for booster or upper-stage application, exhibit inherent decrements in performance at off-design conditions.

The plug nozzle and expansion-deflection (E-D) nozzle are advanced concepts that attempt to achieve this off-design improvement by free expansion of the nozzle flow to ambient conditions. The distinction between the plug and the E-D nozzle lies in the method of freely expanding the nozzle flow (see fig. 1). In the case of a plug nozzle, the

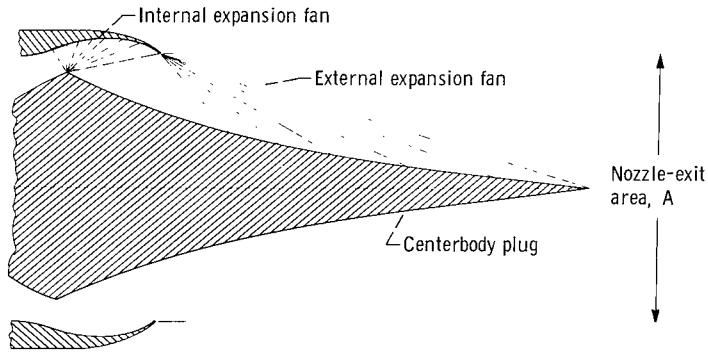

(a) Plug nozzle.

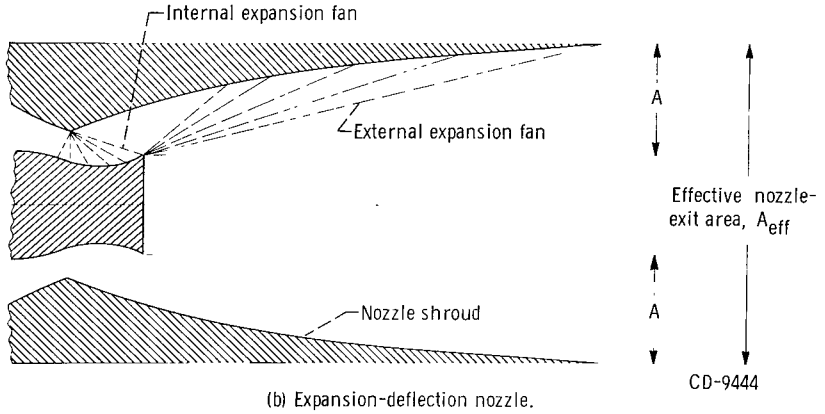

(b) Expansion-deflection nozzle.

Figure 1. - Annular plug and expansion-deflection nozzle concepts.

free-expansion boundary is external to the nozzle, and a centerbody or plug transmits the pressure forces. For the E-D nozzle, the free-expansion boundary is inside the nozzle, and a shroud transmits the pressure forces. The propulsion system may take the form of convergent-divergent (C-D) thrusters clustered around a centerbody or an integration of this cluster into a single annulus or a modular annulus (see refs. 1 and 2 for a more complete description of these conceptual variations.).

This report presents the results of an experimental study concerning the performance of annular plug and E-D nozzles. The study was a continuation of work previously done at the Lewis Research Center (ref. 3). Models that used dried air at a chamber pressure of 1000 psi (6.895×10^6 N/m^2) were tested for quiescent performance in the 10- by 10-foot (3.05- by 3.05-m) supersonic wind tunnel of the Lewis Research Center utilizing the altitude variation capability of this facility. External flow effects were studied in the transonic test section of the 8- by 6-foot (2.44- by 1.83-m) supersonic wind tunnel of the Lewis Research Center. Mach numbers ranged from 0.56 to 2.0. Geometry variations included plug length and internal expansion. The effects of base bleed were also studied.

SYMBOLS

A	nozzle-exit area
A_{eff}	effective nozzle-exit area
A^*	nozzle-throat area
C_D	drag coefficient, $D/P_c A^*$
C_F	thrust coefficient, $F/P_c A^*$
D	drag
F	measured nozzle thrust
F_i	ideal thrust of primary-plus secondary-nozzle flow
ΔF	decrement of thrust
h	altitude
M_{ex}	Mach number at nozzle exit
M_{lip}	Mach number at lip station
M_0	free-stream Mach number
P_c	nozzle total pressure
p_b	average base pressure

p_0 free-stream static or ambient pressure

T_p total temperature of primary flow

T_s total temperature of secondary flow

w_p primary weight flow

w_s secondary weight flow

γ ratio of specific heats

APPARATUS

Thrust and Flow Measuring Systems

The models were strut mounted in both test facilities, as shown in figure 2 for the full-length isentropic plug nozzle configuration. A schematic drawing of the model internal geometry and the thrust measurement system is shown in figure 3. The model external shell was grounded and was supported from the tunnel ceiling by a hollow, vertical strut. The nozzle portion of the model was attached to the primary and secondary air bottles, which were cantilevered by flow tubes from supply manifolds located outside

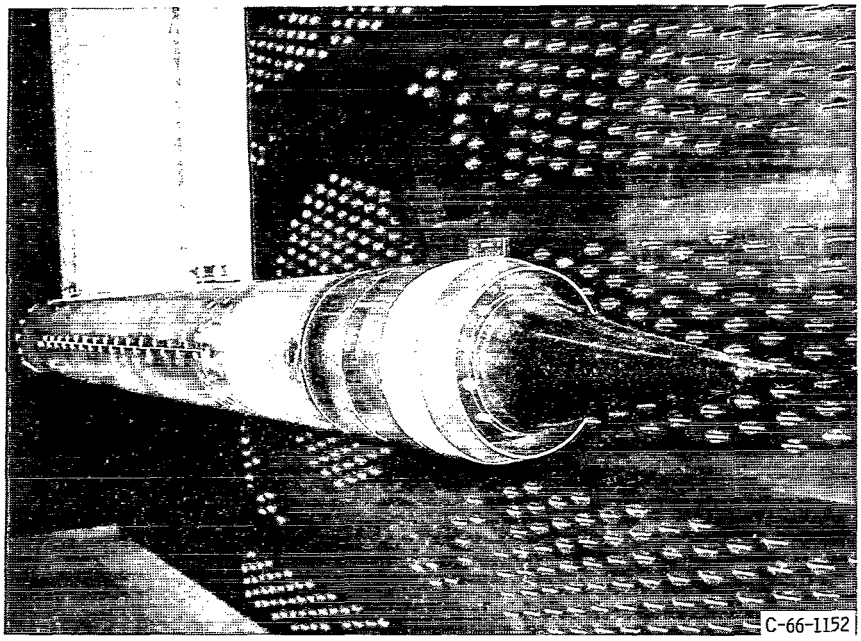

Figure 2. - Full-length plug nozzle mounted in 8- by 6-foot wind tunnel.

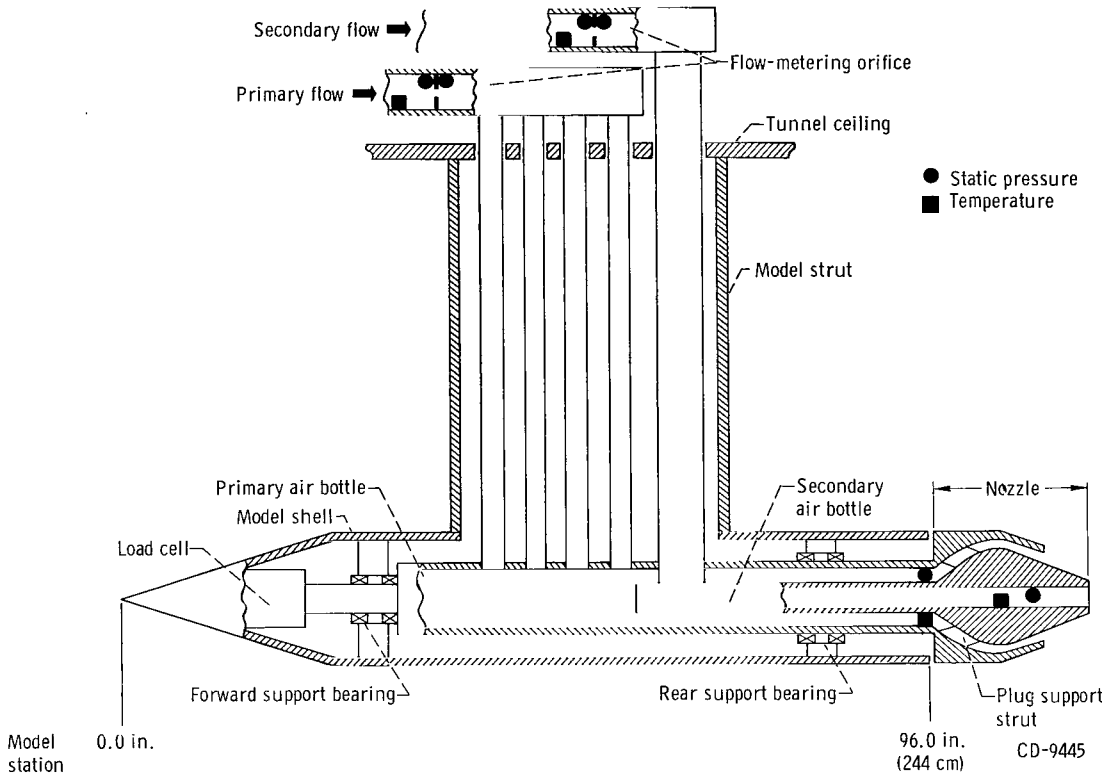

Figure 3. - Schematic of model internal geometry and thrust measuring system.

the test section. Front and rear bearings supported the primary air bottle. The secondary air line, which passed through the plug, was supported by struts attached to the nozzle outer shroud. Thus, the nozzle axial force, including secondary flow effects, was transmitted to the load cell in the nose of the model shell. Since the floating part of the model included a portion of the forward section of the afterbody and the boattail, the measured axial force represented the installed nozzle value of thrust minus drag.

A static calibration of the thrust measuring system was obtained by applying a known force to the nozzle and measuring the output of the load cell. To minimize changes in the calibration due to variations in temperature (e.g., aerodynamic heating due to external flow), the load cell was surrounded by a water-cooled jacket and was maintained at a constant temperature.

As indicated by figure 3, primary and secondary flow rates were obtained by means of standard ASME flow-metering orifices located in the external supply lines. The total pressure of the primary and secondary air at the nozzle station was calculated from the continuity equation, the measured weight flow, and the static pressure and temperature measurements located within the air bottles as shown.

Nozzle Geometry

Nozzle geometry details are presented in figure 4. All nozzle configurations tested were based on the following design criteria: A full-scale vehicle, typical of a post-Saturn booster, was assumed to be approximately 75 feet (22.9 m) in diameter with a takeoff thrust of approximately thirty million pounds (1.33×10^8 N). The propulsion system would have a chamber pressure of 1000 psia (6.895×10^6 N/m^2), and the products of combustion would have a ratio of specific heats γ of 1.2. With most of the advanced nozzle concepts, internal expansion would be utilized to expand the flow to ambient pressure at sea level ($P_c/p_0 = 68$). It would be desirable to use the entire base area of the vehicle for external expansion. However, this cannot be done with plug nozzles because of the inherent boattail surface. Therefore, it was assumed that only 80 percent of the

X		R_1		R_2	
in.	cm	in.	cm	in.	cm
0	0	0	0	0	0
2.963	7.53	.463	1.176		
3.500	8.89	.552	1.402		
4.000	10.16	.633	1.608		
4.500	11.43	.715	1.816		
5.000	12.70	.800	2.032		
5.500	13.97	.896	2.275		
6.000	15.24	.989	2.512		
6.500	16.51	1.081	2.748		
7.000	17.78	1.178	2.992		
7.500	19.05	1.281	3.255		
8.000	20.31	1.389	3.522		
8.500	21.58	1.507	3.830		
9.000	22.87	1.631	4.144		
9.500	24.13	1.763	4.479		
10.250	26.03	1.987	5.048		
13.074	33.21			3.764	9.565
13.500	34.30			3.811	9.680
14.000	35.58			3.926	9.970
14.500	36.83			4.024	10.022
15.000	38.11			4.092	10.39
15.500	39.38			4.120	10.46
16.000	40.65			4.076	10.35
16.344	41.50	3.804	9.66		
16.415	41.70			3.886	9.865
16.647	42.29	3.447	8.75		
16.890	42.91			3.604	9.155
16.930	43.00	2.950	7.495		
17.345	44.05			3.430	8.710

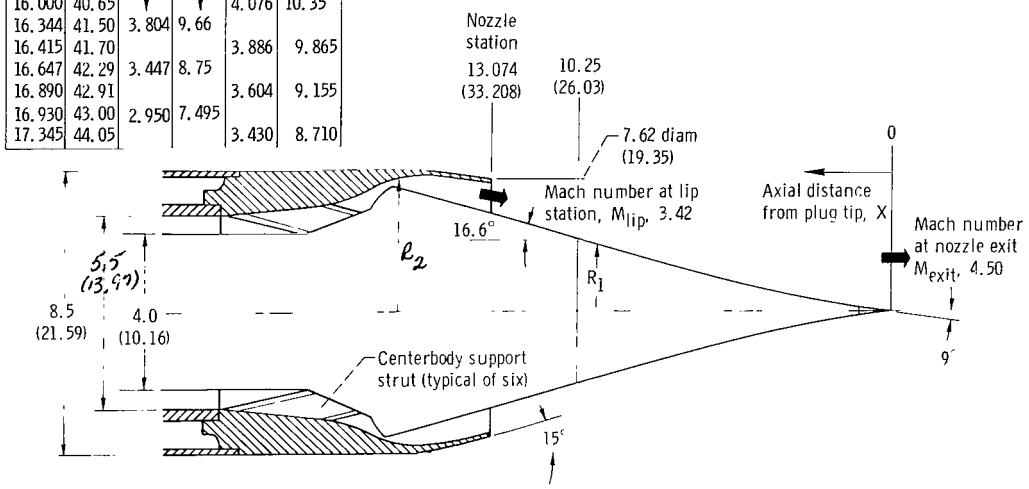

(a) Full-length isentropic plug nozzle.

Figure 4. - Nozzle geometry details. All dimensions are in inches (cm).

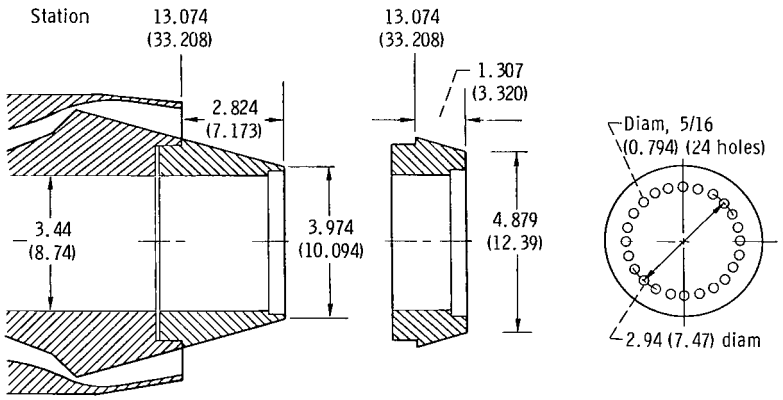

(b) Truncated plug nozzles. Exit plane of 0-percent plug located at station 13.074 inches (33.208 cm).

X		R_1		R_2	
in.	cm	in.	cm	in.	cm
0	0	3.42	8.685	3.7	9.400
.039	.099			3.819	9.680
.052	.132	3.510	8.920		
.077	.196	3.570	9.070		
.108	.274	3.665	9.280		

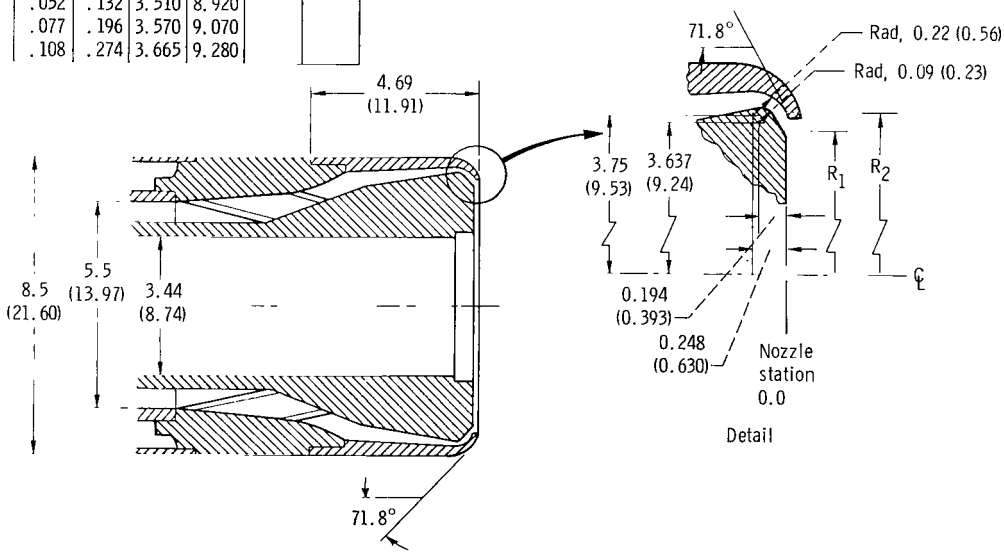

(c) 0-Percent-length plug nozzle with no internal expansion.

Figure 4. - Continued.

X		R_1		X		R_2	
in.	cm	in.	cm	in.	cm	in.	cm
0	0	4.250	10.79	6.108	15.52	2.075	5.276
1.7	4.32	4.101	10.41	6.510	16.53	1.974	5.015
2.1	5.335	4.062	10.31	6.912	17.55	1.886	4.791
2.504	6.36	4.012	10.19	7.314	18.56	1.812	4.603
2.896	7.355	3.950	10.09	7.715	19.59	1.757	4.463
3.136	7.97	3.902	9.91	8.116	20.60	1.718	4.363
9.593	24.38	2.202	5.60	8.518	21.61	1.712	4.350
9.791	24.88	2.451	6.23	8.920	22.65	1.746	4.437
9.944	25.27	2.726	6.92	9.322	23.68	1.846	4.690
10.108	25.68	3.122	7.93	9.724	24.70	2.078	5.275
10.438	26.49	3.452	8.77	9.969	25.31	2.256	5.730
10.768	27.34	3.500	8.89	10.258	26.10	2.386	6.060
11.550	29.32	3.500	8.89	10.418	26.46	2.438	6.195
				10.634	27.00	2.450	6.220
				11.550	29.35	2.450	6.220

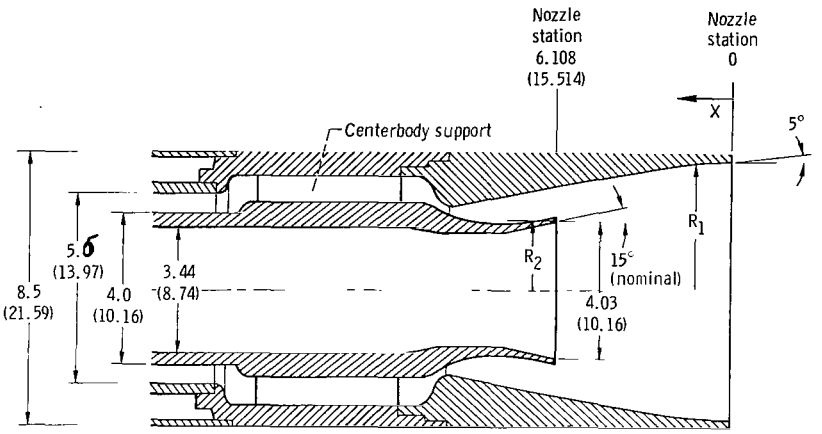

(d) Expansion-deflection nozzle.

X		R	
in.	cm	in.	cm
0	0	3.7	9.40
9.935	25.22	1.038	2.64
10.883	27.62	.914	2.32
13.308	33.80	1.832	3.65
15.732	39.95	2.75	6.98
17.2	43.70	2.75	6.98

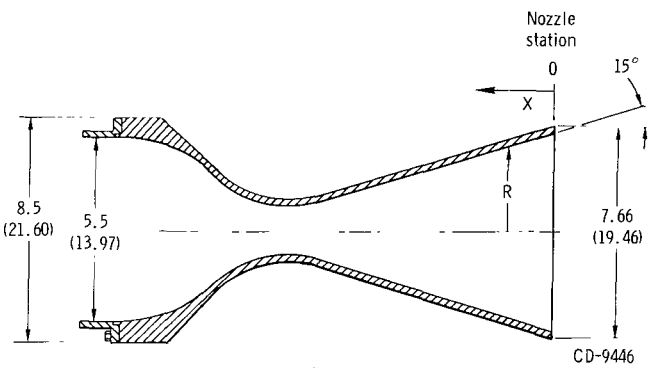

(e) Convergent-divergent nozzle.

Figure 4. - Concluded.

base could be used for external expansion, resulting in a design total- to ambient-pressure ratio of 290.

The model was 8.5 inches (21.6 cm) in diameter, which is approximately 1 percent of full scale. Since cold air (γ = 1.4) was used for the nozzle flow, the full-scale γ could not be simulated. Instead, the model internal and overall area ratios were selected to match the design pressure ratios of the full-scale vehicle (i.e., P_c/p_0 = 68 for the internal expansion and P_c/p_0 = 290 for the overall area ratio). Thus, the cold-flow nozzle area ratios were substantially less than those of the assumed vehicle.

Details of the full-length isentropic plug are shown in figure 4(a). Internal expansion, assumed for the full-scale vehicle, was provided to reduce the nozzle pressure from 1000 psia (6.895×10^6 N/m^2) in the chamber to 14.7 psia (1.013×10^5 N/m^2) at the nozzle exit for sea-level takeoff (P_c/p_0 = 68). The resultant internal area ratio was 6.3, and the average Mach number at the lip, station 13.074 inches (33.208 cm), was 3.42.

The expansion fan emanating from the corner at the throat was cancelled by the contour of the opposite wall, thereby providing uniform flow at the discharge. The parabolic contour of this wall was determined by the approximate techniques of reference 4. As ambient pressure decreases, the flow expands externally about the cowl lip and becomes fully expanded at a pressure ratio of 290. Thus, the overall design area ratio was 16.56, and the exit Mach number was 4.5. The plug shape was conical from the throat to station 10.25 inches (26.03 cm), which is the intersection point of the initial Mach line emanating from the nozzle lip. The remaining external plug shape was designed, with the use of the method presented in reference 5, to provide uniform parallel flow at the exit station. This shape is partially isentropic with a finite cone angle (18°) at the tip. (Nozzle coordinates are presented in fig. 4(a).)

A conical boattail with an angle of 15° was used. This angle is related to the Prandtl-Meyer turning angle between the lip Mach number of 3.42 and the exit Mach number of 4.50. The projected area of the boattail was about 20 percent of the maximum model area.

Details of the truncated plug nozzles are shown in figure 4(b). The full-length plug has the obvious disadvantage of excessive length, which will cause cooling and structural problems. Truncating the plug, although desirable, should result in reduced nozzle performance because of divergence losses (due to nonaxial discharge) and losses in plug pressure forces. However, some of these losses may be compensated by gains in base pressure forces, which result from the flow field established in the base of the truncated plug because of the recirculation of the nozzle exhaust flow. This phenomenon is well known and has been discussed in references 6 to 11. Furthermore, reference 6 indicates that small amounts of bleed flow into the base can result in a significant increase in the base pressure. In flight, this bleed or secondary flow could possibly be obtained by utilizing the turbopump discharge gases.

Plug lengths considered were 21, 10, and 0 percent of the full-plug length between the nozzle lip and the plug tip. The 21-percent length was chosen because this length contains only the simple conical portion of the external plug surface. The 0-percent length was chosen to determine the effect of not having a plug surface extending beyond the lip station. The 10-percent length was an arbitrary length midway between the 0- and 21-percent lengths.

Two base bleed configurations were studied. The open base consisted of a fully open passage with an inside diameter of 3.44 inches (8.74 cm). The perforated base configuration consisted of a metal base plate covering the secondary flow passage. This plate was perforated with 24 holes, each 5/16 inch (0.794 cm) in diameter, equally spaced about a 2.94-inch (7.47-cm) circle.

An additional truncated plug configuration that was tested consisted of a 0-percent-length plug without internal expansion. This configuration, shown in figure 4(c), is a

concept that attempts to utilize the base pressure phenomenon to compensate for the elimination of both the plug surface and the internal expansion. The nozzle flow is discharged at sonic velocities and expanded through an area ratio of 16.56, based on the projected lip diameter. Since the flow must be axial at the design point, as was noted for the full-length plug, the inclination of the throat was fixed at an angle of 71.8° to the centerline. For a sonic discharge velocity, this throat inclination results in a steep boattail angle, also 71.8°. When compared with the 15°-boattail angle of the other truncated plug nozzles, it is evident that internal expansion can provide low boattail angles to minimize external drag. (Nozzle coordinates for this configuration are presented in fig. 4(c).) The secondary bleed flow passage was identical to that of the truncated plug.

Details of the E-D nozzle are shown in figure 4(d). The E-D nozzle features a cylindrical afterbody. The boattail area of the plug nozzle is eliminated but appears as the center base area in the E-D nozzle. Internal expansion again was provided to reduce the nozzle pressure from 1000 psia (6.895×10^{6} N/m^2) in the chamber to 14.7 psia (1.013×10^{5} N/m^2) at the discharge of the internal expansion, station 6.108 inches (15.52 cm). The parabolic contour of the internal expansion was determined by the approximate technique of reference 4 (as was done for the plug nozzles) to provide uniform parallel flow at the discharge. As ambient pressure decreases, the flow expands externally about the lip of the discharge. The parabolic internal contour of the skirt, also determined by the technique of reference 4, cancelled the emanated expansion fan so that uniform parallel flow resulted at the exit plane for the same pressure ratio ($P_c/p_0 = 290$) as that of the plug nozzle. (Coordinates for the contours of both the internal and external expansion surfaces are presented in fig. 4(d).) The corresponding area ratio of the E-D nozzle ($A/A^* = 16.56$) was physically equal to the ratio of the annular exit area to the throat area, where the annular area is that between the projected lip diameter at the discharge of the internal expansion and the maximum model diameter (see. fig. 1). Since the effective exit area of the E-D nozzle includes the center base area, a higher effective area ratio of 21.33 is achieved. Thus, the E-D nozzle makes use of the entire base of the vehicle for the expansion of the jet, consequently, the effective design pressure ratio of the E-D nozzle would be higher than that of the plug nozzle, $P_c/p_0 = 420$ as compared with $P_c/p_0 = 290$.

The discharge angle of the secondary flow passage is analogous to the boattail angle of the plug nozzle. The discharge angle was determined from considerations previously mentioned in the discussion of the plug nozzle boattail and was nominally 15°.

The C-D nozzle, shown in figure 4(e), was a conical nozzle with a 15°-discharge angle, designed for the same area ratio as the plug nozzles, 16.56. The C-D nozzle was tested to provide a reference for the relative performance of the advanced nozzles. Furthermore, it was used to check the model thrust and weight flow measuring systems

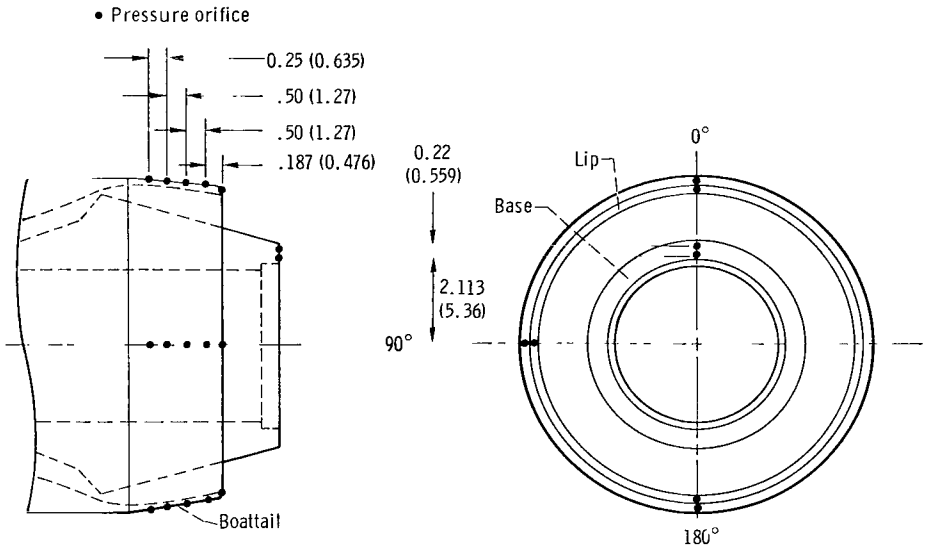

(a) 10-Percent plug length.

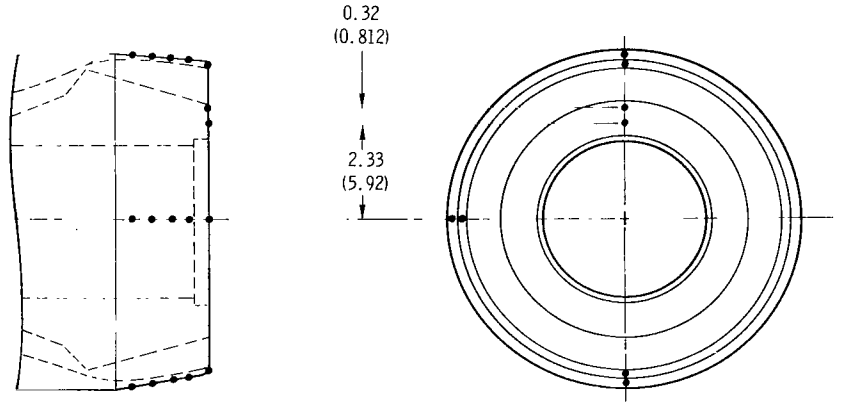

(b) 0-Percent plug length.

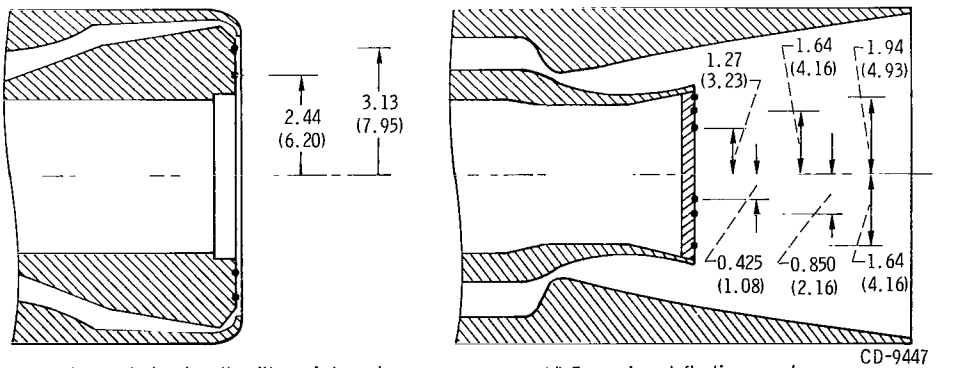

(c) 0-Percent plug length with no internal expansion.

(d) Expansion-deflection nozzle.

Figure 5. - Boattail and base instrumentation details. All dimensions are in inches (cm).

since the theoretical performance of the C-D nozzle could be predicted by established techniques. Coordinates are presented in figure 4(e).

Boattail and base-plate instrumentation details are shown in figure 5. The boattail instrumentation (fig. 5(a)) was common to all plug nozzle configurations with internal expansion. It consisted of static pressure orifices located on the top, bottom, and side of the boattail surface. These orifices were used to yield the boattail drag by pressure-area integration. Static pressure orifices on the base or lip of the boattail surface gave the nozzle lip pressure for determining the overexpansion loss of the nozzle as well as the pressure force, called lip drag.

Pressures on the base of the truncated plug were determined from orifices located at positions shown in figures 5(a) and (b) for the 10- and 0-percent plug lengths, respectively. Base pressures were not obtained for the 21-percent length. Base pressure instrumentation for the 0-percent plug length without internal expansion and for the E-D nozzle is shown in figures 5(c) and (d), respectively. For the E-D nozzle, the pressure orifices were located on the perforated base plate.

PROCEDURE

A trajectory, typical of the post-Saturn vehicle assumed for the nozzle design, was used to determine the model nozzle total- to ambient-pressure ratio (hereinafter called the nozzle pressure ratio), as a function of Mach number. This trajectory is presented in figure 6 along with the resultant schedule of the nozzle pressure ratio. The model quiescent performance was obtained in the 10- by 10-foot (3.05- by 3.05-m) supersonic wind tunnel. This facility has the capability of quiescent altitude variation from sea level

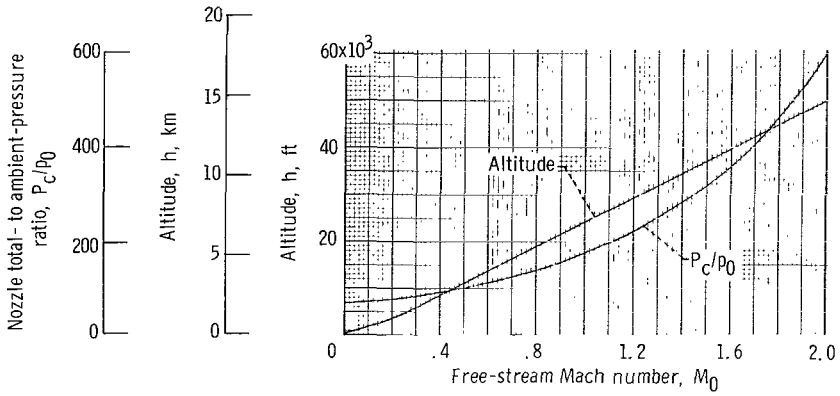

Figure 6. - Assumed vehicle trajectory and nozzle pressure ratio schedule.

to 60 000 feet (18.3 km). The nozzle chamber pressure was maintained at 1000 psia (6.895×10^6 N/m^2) with exceptions to be noted, and the tunnel pressure was varied to obtain nozzle performance over the desired range of pressure ratios. Performance with external flow was obtained in the transonic test section of the 8- by 6-foot (2.44- by 1.83-m) supersonic wind tunnel, which has an altitude variation with Mach number lower than that of the assumed trajectory. Therefore, the nozzle chamber pressure was increased so that the nozzle performance could be obtained at the appropriate pressure ratio for free-stream Mach numbers of 0.56, 0.80, 1.00, 1.37, and 1.97.

RESULTS AND DISCUSSION

Quiescent Performance With No Secondary Flow

Nozzle quiescent performance without secondary flow is presented in figure 7. The ratio of measured thrust to ideal thrust F/F_i (hereinafter called nozzle efficiency) is plotted as a function of the nozzle pressure ratio. The ideal thrust was based on the measured primary weight flow and the nozzle pressure ratio. When secondary flow was used, the ideal thrust also included the ideal thrust of the secondary flow, based on the measured secondary weight flow and the computed secondary total- to ambient-pressure ratio.

The performance of the 15°-conical C-D nozzle is shown in figure 7(a). Maximum data scatter observed was about ±0.5 percent and is an indication of the data repeatability. The curve through the data is a semitheoretical prediction of the nozzle performance. The shape is determined by the theoretical overexpansion and underexpansion losses; however, the level has been adjusted to match the measured performance at the design point. At off-design pressure ratios, the measured data agree well with the calculated trend. As expected, the maximum efficiency occurred at the design point ($P_c/p_0 = 290$), and the mean value was 0.978. The theoretical divergence loss for the 15°-conical C-D nozzle is 0.017, and the resultant theoretical maximum efficiency is 0.983, neglecting friction. The measured nozzle efficiency agreed substantially with the theoretical value, which indicates the accuracy of the measured data.

The performance of the full-length plug nozzle is presented in figure 7(b). Data for pressure ratios of less than 68 were obtained at reduced chamber pressure. Semitheoretical performance curves are presented for C-D nozzles with area ratios of 6.3 and 16.56 and were calculated by the same method used for the C-D nozzle in figure 7(a). The experimental data agree well with the calculated curves. Qualitatively, therefore, it appears that the plug nozzle performance at low pressure ratios is similar to that of a C-D nozzle with the same area ratio as the plug nozzle internal expansion. At high pres-

sure ratios, the performance is similar to that of a C-D nozzle with an area ratio equal to the plug nozzle overall area ratio. The transition from one curve to the other occurs in the region of nozzle pressure ratios where the relative significance of external expansion increases. Quantitatively, the plug nozzle performance was better than the performance of the C-D nozzle (presented in fig. 7(a)) at all nozzle pressure ratios. The most significant difference in performance occurred between sea level and the design pressure ratio of 290. For example, at $P_c/p_0 = 68$, the plug nozzle efficiency was 0.984 and the C-D nozzle efficiency was 0.928. At $P_c/p_0 = 290$, the plug nozzle efficiency was 0.99, whereas the C-D nozzle efficiency was 0.978. This higher efficiency of the plug nozzle at high pressure ratios can be attributed to the elimination of any divergence loss. It can be seen that the plug nozzle has a nearly constant and optimum performance at all altitudes and provides the desired altitude compensation.

The performances of the truncated plug and E-D nozzles are presented in figure 7(c). Dashed lines are semitheoretical performance curves for the C-D and full-length plug nozzles repeated from figures 7(a) and (b). Symbols denote the measured performance of truncated plug and E-D nozzles. Plug truncation tended to decrease the plug nozzle performance, and this decrement increased with increasing amounts of plug truncation. The performance of the 21-percent plug nozzle was greater than that of the C-D nozzle at all pressure ratios, but was less than that of the full-length plug. Measured nozzle efficiency was 0.983 at the design pressure ratio and 0.964 at sea level. The performances of the 10- and 0-percent plug nozzles were nearly comparable and were less than the C-D nozzle performance, except near sea level. Measured nozzle efficiencies were 0.970 and 0.968 at the design pressure ratio for the 10- and 0-percent plug nozzle, respectively, whereas at sea level the efficiencies were 0.953 and 0.949. Obviously, pressures in the base of the truncated plugs compensate to some extent for the loss in plug surface, and in the case of the 21-percent plug, the resultant nozzle performance was nearly comparable with that of the full-length plug. However, in the case of the 0- and 10-percent plug lengths, significant losses occurred.

Elimination of the internal expansion resulted in a poor nozzle performance; in fact, the 0-percent plug nozzle without internal expansion was not even comparable with the C-D nozzle. The nozzle efficiency at sea level was 0.847 and the efficiency at the design pressure ratio was 0.898. Evidently, the base pressure forces do not adequately compensate for the losses incurred by eliminating both the plug surface and internal expansion. The high discharge angle inherent in this configuration requires that the nozzle flow turn to an axial direction through an oblique shock. Presumably, nozzle performance could be improved by utilizing a partial plug to turn the flow.

The E-D nozzle performance was generally comparable with that of the C-D nozzle rather than with that of the full-length plug. Evidently, the E-D nozzle was not altitude compensating. Below $P_c/p_0 = 290$, the E-D nozzle performance was less than that of the

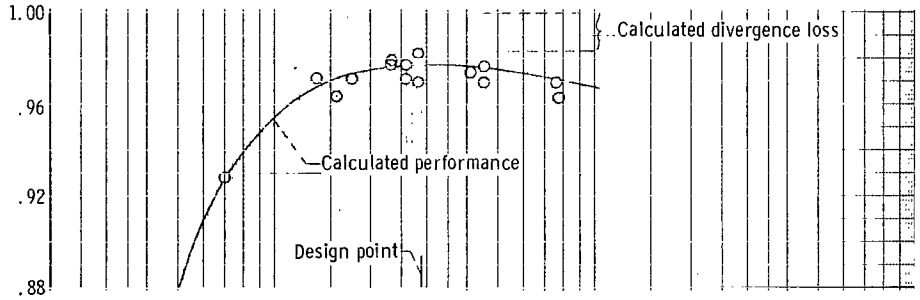

(a) 15°-Conical convergent-divergent nozzle. Nozzle area ratio, 16.56.

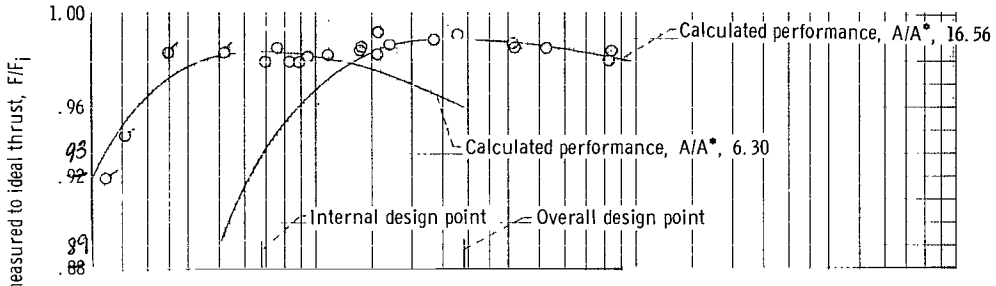

(b) Full-length isentropic plug nozzle. Tailed symbols denote chamber pressure less than 1000 pounds per square inch absolute (6.895×10^6 N/m^2).

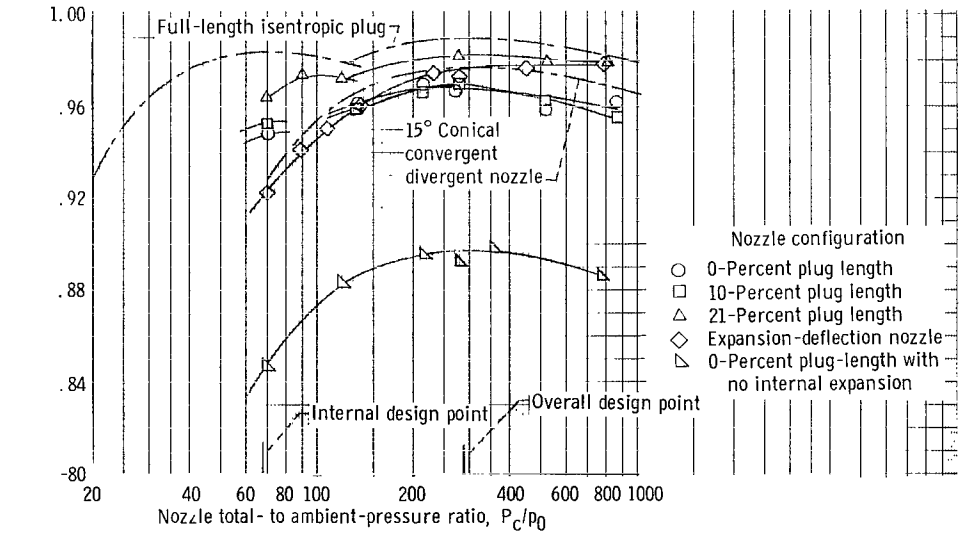

(c) Truncated plug and expansion-deflection nozzles.

Figure 7. - Nozzle quiescent performance without secondary flow.

C-D nozzle, but at higher nozzle pressure ratios, the E-D performance was greater. This apparent gain is due to the fact that the effective design point of the E-D nozzle (previously discussed in the section Nozzle Geometry) is higher than the design point of the C-D nozzle. A comparison was made of the E-D nozzle performance with that of a C-D nozzle having an area ratio of 21.33 (not presented herein). The 21.33-C-D nozzle performance was calculated by the semitheoretical method used for the 16.56 C-D nozzle; the measured efficiency of the E-D nozzle at $P_c/p_0 = 420$ was assumed as the design point efficiency of the 21.33 C-D nozzle. The E-D performance was generally comparable with that of the 21.33 C-D nozzle, except near sea level, where the E-D performance was higher. However, a 21.33 C-D nozzle may be separated near sea level, and the actual performance would be higher than calculated, making the E-D and 21.33 C-D nozzles more comparable.

A comparison of base pressures for the truncated plug nozzles (with and without internal expansion) and for the E-D nozzle is shown in figure 8 for the case of no secondary flow. Average base- to ambient-pressure ratio is plotted as a function of nozzle pressure ratio. The base pressure of both nozzle types results from the same phenomenon, the flow field established by recirculation of the annular nozzle exhaust flow. Yet,

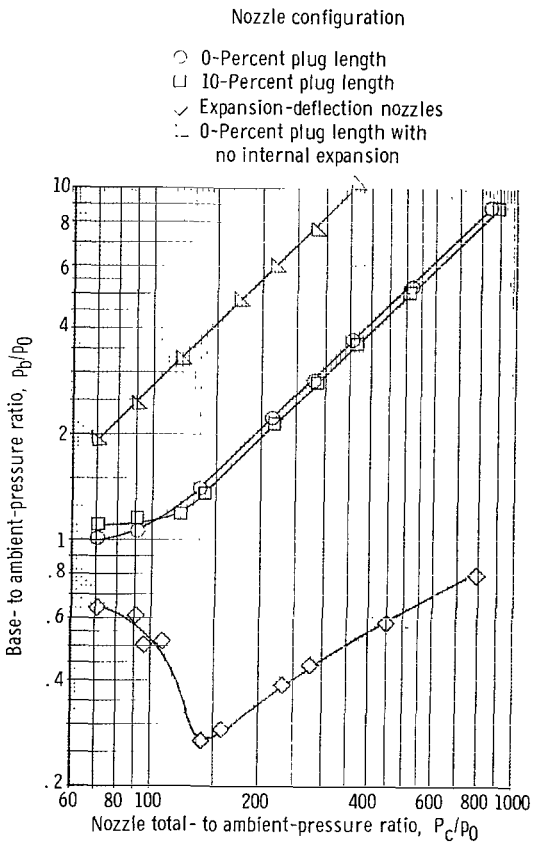

Figure 8. - Comparison of base pressures for truncated plug and expansion-deflection nozzles with no secondary flow.

the variation with nozzle pressure ratio is significantly different. Base pressures for the truncated plug nozzles were always greater than ambient pressure. Hence, the resultant base force adds to the nozzle thrust.

The 0-percent plug without internal expansion had significantly higher base pressures than those for the other truncated plug nozzles, which is a result of the high discharge angle of the configuration. However, as shown in figure 7(c) the resultant base force did not compensate for eliminating the plug and internal expansion. In contrast, base pressures for the E-D nozzle were always less than ambient; hence, the resultant force represents a drag and reduces the nozzle thrust. Furthermore, since the nozzle flow expands to base pressure rather than to ambient pressure, the nozzle shroud pressures overexpand, resulting in reduced efficiency. Clearly, base drag and overexpansion are responsible for the lack of altitude compensation in the E-D nozzle.

The variation of E-D nozzle base pressure can be explained as follows. At nozzle pressure ratios near sea level, the annular nozzle flow acts as an ejector and aspirates the base, producing base pressures less than ambient. As ambient pressure decreases (increasing nozzle pressure ratio), jet expansion results in a stronger recirculated flow field and in a decrease in base aspiration. Thus, for $P_c/p_o \gtrsim 135$, the base pressure ratio increased with nozzle pressure ratio. At some nozzle pressure ratio, the base will become pressurized and the base pressure will exceed ambient, resulting in a gain in E-D performance due to base thrust. This nozzle pressure ratio was apparently higher than those tested.

The effective design pressure ratio of the E-D nozzle would be defined as that nozzle pressure ratio above which the base pressure remains constant. Above this nozzle pressure ratio, an increase in base pressure ratio results from a decrease in ambient pressure, and the curve of the base pressure ratio is characterized by a straight line with a slope of 1.0. When this condition exists, the base flow field is said to be "choked." The E-D curve indicates that this choking condition was not the case for the range of nozzle pressure ratios tested. The performance curve (fig. 7(c)) substantiates these test results, in that it apparently had not peaked.

Quiescent Performance With Secondary Flow

The variation of nozzle quiescent performance with secondary flow is shown in figure 9 for both the open and perforated base. The nozzle efficiency is plotted as a function of the corrected secondary-to-primary weight flow ratio $(W_s/W_p)\sqrt{T_s/T_p}$. The parametric variation with nozzle pressure ratio is shown also. Since the primary and secondary air were at the same temperature during the model test, $T_s/T_p = 1$ and the corrected weight flow ratio was numerically equal to the actual weight flow ratio. Nozzle perfor-

mance for the 21-percent plug is presented in figure 9(a). In general, small amounts of secondary flow $\left[(W_s/W_p)\sqrt{T_s/T_p} < 0.02\right]$ improved performance at pressure ratios less than design. Larger amounts of bleed resulted in a decreasing trend, particularly for the perforated base configuration. Furthermore, the performance of the perforated base configuration with large flow rates was generally lower than that of the open base over the entire range of nozzle pressure ratios.

Performance of the 0- and 10-percent plug nozzles is presented in figure 9(b). Secondary flow increased nozzle performance for both configurations and had more effect than was seen for the 21-percent plug nozzle. Small amounts of bleed again produced the largest increase in performance, and large amounts of secondary flow resulted in a decreasing trend.

The performance of the 0-percent plug nozzle without internal expansion is presented in figure 9(c). As was noted for the configurations with internal expansion, small amounts of bleed increased nozzle performance. However, for both the open and perforated base, increasing secondary flow rate resulted in a generally increasing efficiency over the full range of secondary flow rates rather than in peaking at low flow rates. Noz-

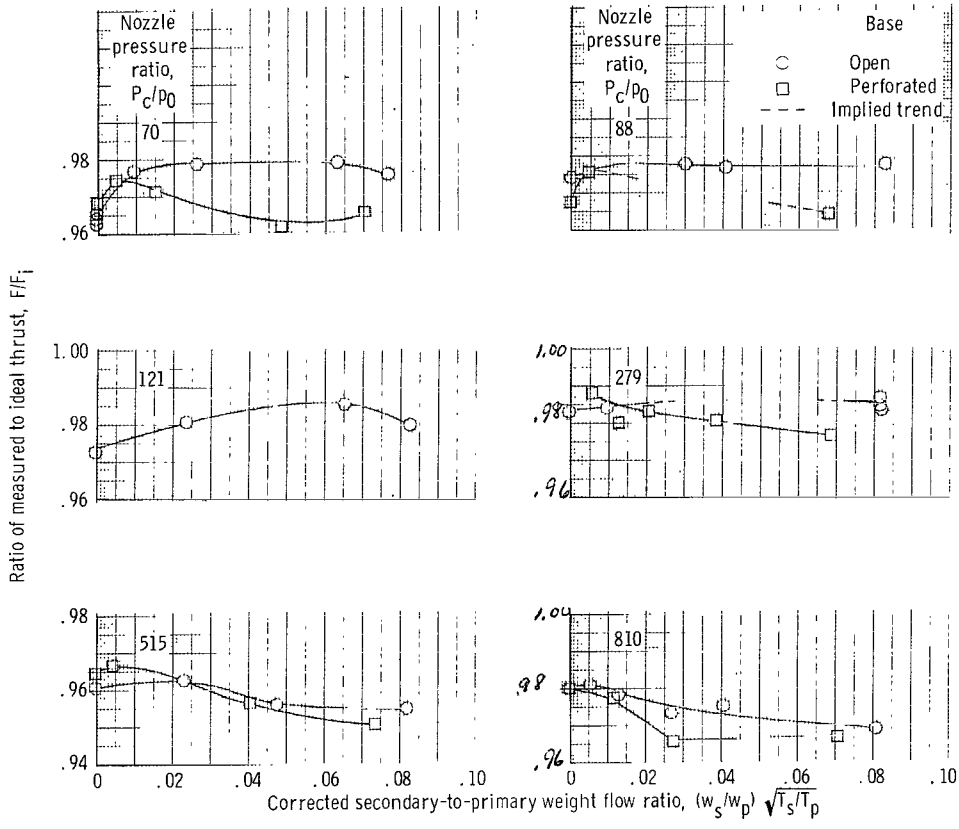

(a) 21-Percent-length isentropic plug.

Figure 9. - Nozzle quiescent performance with secondary flow.

zle efficiencies for the perforated base were generally less than those for the open base, particularly for large flow rates.

The performance of the E-D nozzle is shown in figure 9(d). For the open base configuration, secondary flow generally increased nozzle efficiency over the full range of flow rates and nozzle pressure ratios. However, large flow rates for the perforated base resulted in decreasing nozzle performance and in lower efficiencies than those of the open base.

A comparison of the quiescent performance of truncated plug and E-D nozzles as affected by a small amount of secondary flow is presented in figure 10. Nozzle efficiencies were determined from figure 9 for $(W_s/W_p)\sqrt{T_s/T_p} = 0.015$. It was assumed that on the

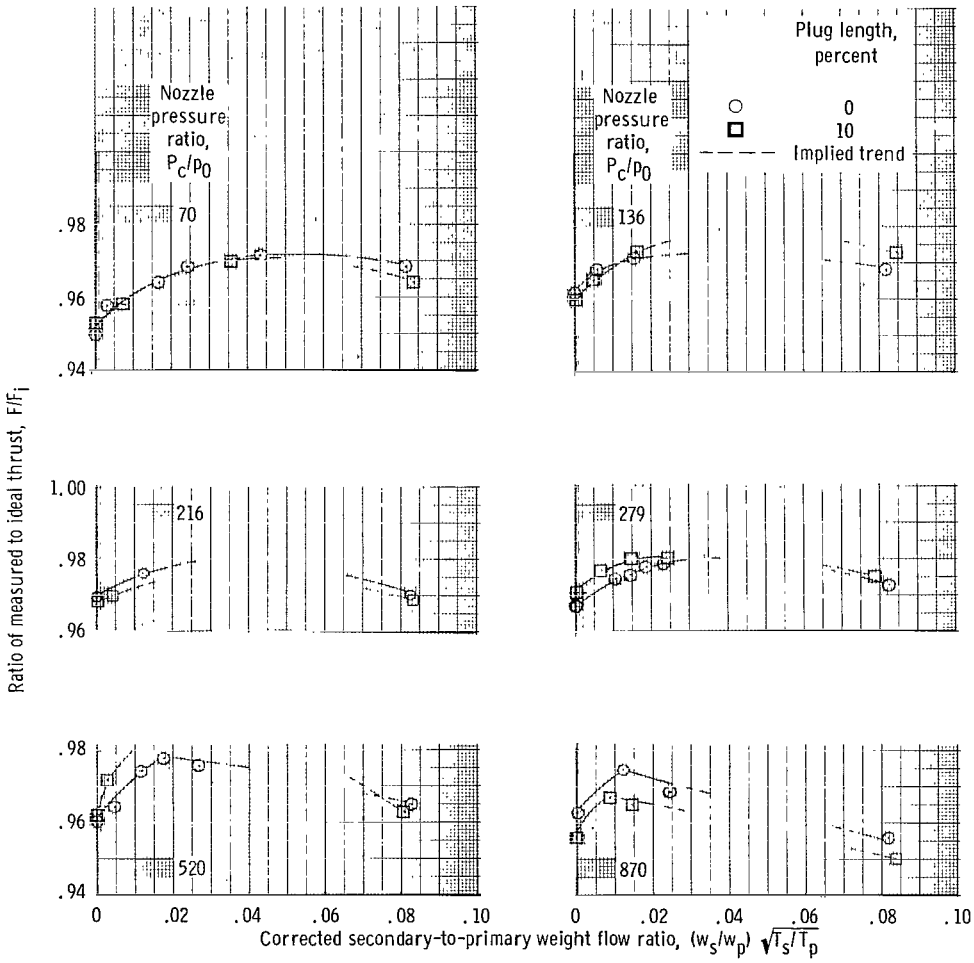

(b) 0- and 10-Percent-length isentropic plug nozzles with open base.

Figure 9. - Continued.

full-scale vehicle the turbopump exhaust would be utilized as the secondary flow and that, for large thrusters of the F-1 or M-1 class, the corrected secondary-to-primary weight flow ratio is typically 0.015. As expected, this small amount of secondary weight flow increased the performance of all configurations. The performance of the 21-percent plug nozzle was more comparable with that of the full-length plug, and the performance of both the 0- and 10-percent plug nozzles was greater than or comparable with that of the C-D nozzle. However, the performance of the 0-percent plug nozzle without internal expansion, although improved, could not compare with that of the C-D nozzle. Referring to

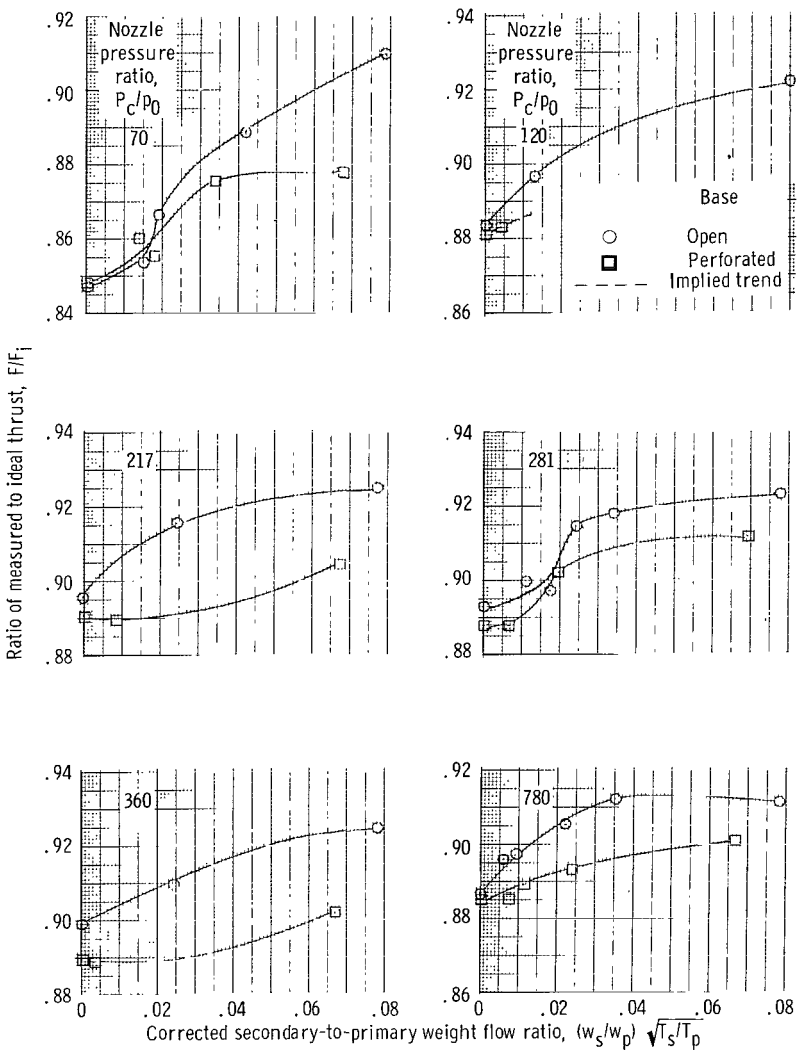

(c) 0-Percent plug length with no internal expansion.

Figure 9. - Continued.

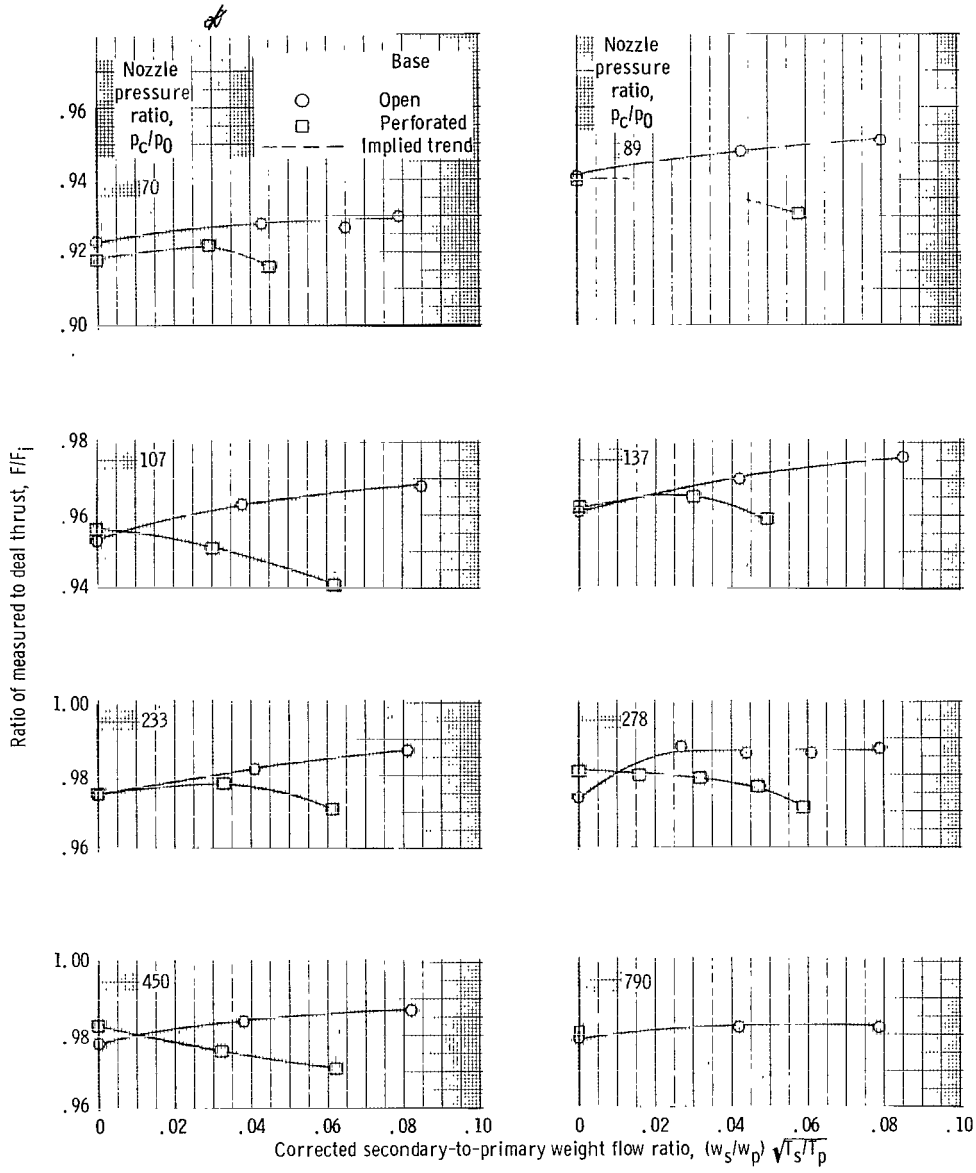

(d) Expansion-deflection nozzle.

Figure 9. - Concluded.

* see errata sheet

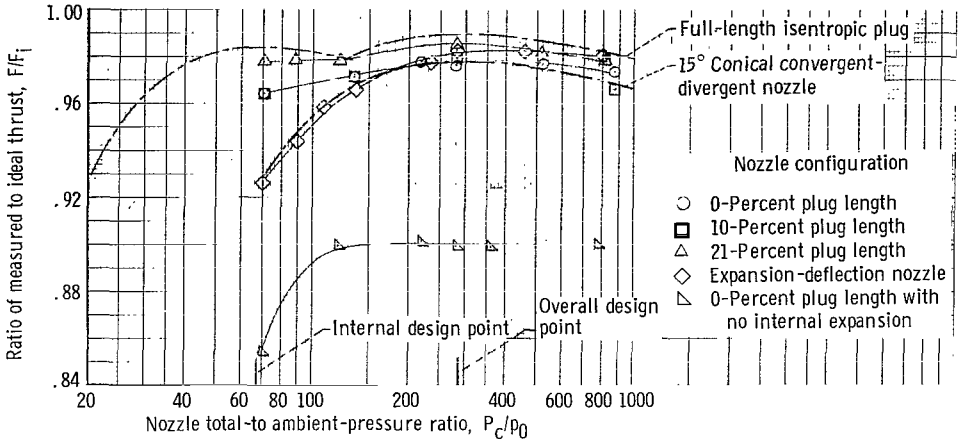

Figure 10. - Comparison of nozzle quiescent performance with corrected secondary-to-primary weight flow ratio of 0.015 and open base.

figure 9(c), it can be seen that flow rates as high as $(W_s/W_p)\sqrt{T_s/T_p} = 0.08$ would not produce the desired improvement. The E-D nozzle performance was better only at nozzle pressure ratios above the C-D nozzle design point.

The effect of secondary flow on truncated plug and E-D nozzle base pressures is shown in figure 11. Base pressure ratio plotted as a function of corrected secondary-to-primary weight flow ratio is presented in figure 11(a) for the 0- and 10-percent plug nozzles, in figure 11(b) for the 0-percent plug without internal expansion, and in figure 11(c) for the E-D nozzle. In the case of the truncated plugs, base pressure increased significantly for small amounts of secondary flow, as was expected, and thus correlated with the observed increase in nozzle efficiency for small flow rates. However, base pressure for the E-D nozzle indicated little effect of secondary flow, except for an increase at high flow rates and nozzle pressure ratios.

Figure 12 presents a comparison of base pressures for the truncated plug and E-D nozzles at a corrected secondary-to-primary weight flow ratio of 0.015 and corresponds to the comparison of nozzle efficiency presented in figure 10 for the same secondary flow rate. Base pressure ratio is plotted as a function of nozzle pressure ratio, and symbols differentiate between the plug and E-D base pressures. Dashed lines denote data for those configurations without secondary flow that are repeated from figure 8. In general, this small, constant amount of secondary flow increased the truncated plug base pressure ratio by a constant amount, and the base pressures were greater than ambient, indicating an increase in base thrust and nozzle efficiency. However, the E-D nozzle base pressure was only slightly affected by the secondary flow, indicating little effect on the base thrust and nozzle efficiency.

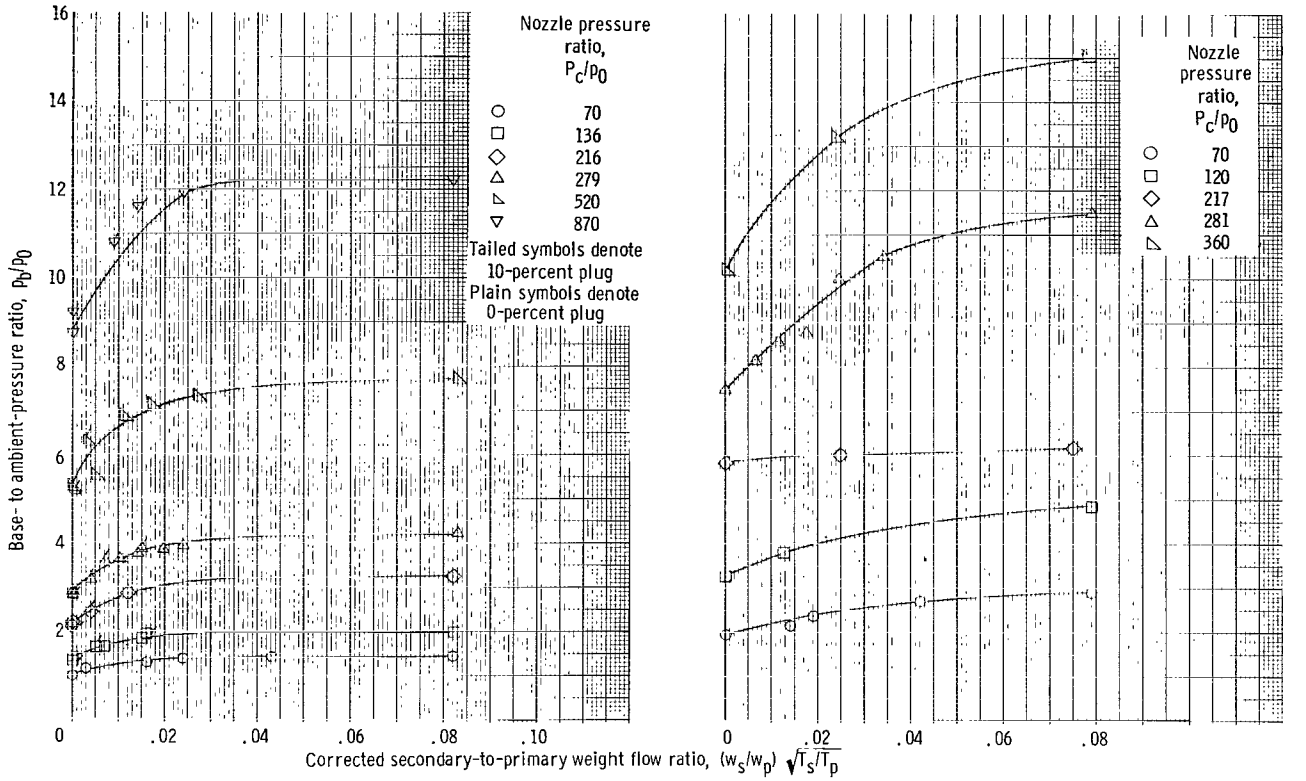

(a) 0- and 10-Percent plug length with open base.

(b) 0-Percent plug length with no internal expansion and open base.

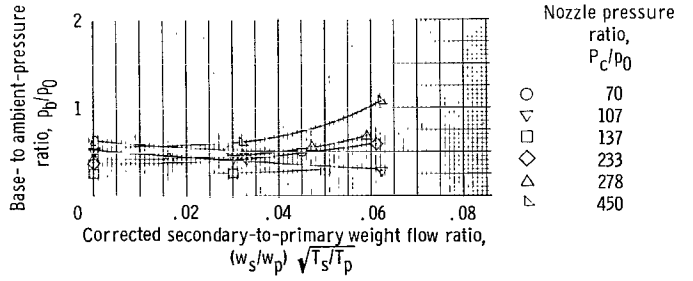

(c) Expansion-deflection nozzle with perforated base.

Figure 11. - Effect of secondary flow on truncated plug and expansion-deflection nozzle base pressures.

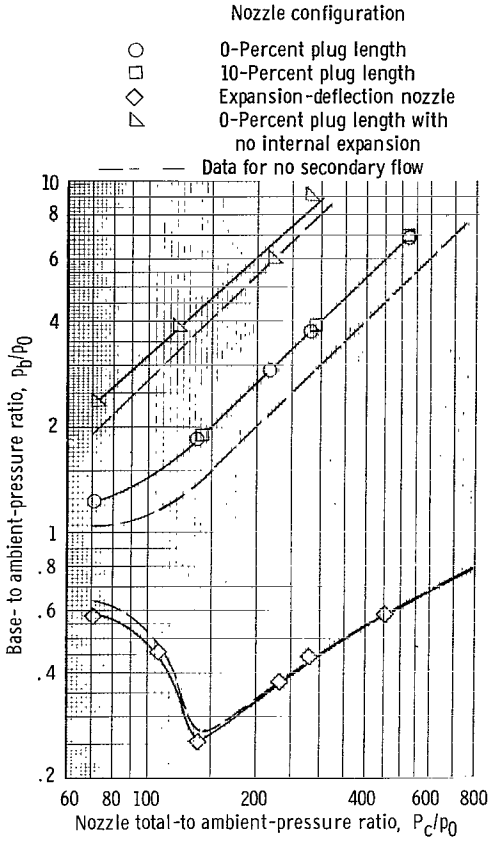

Figure 12. - Comparison of base pressures for truncated plug and expansion-deflection nozzles with open base. Corrected secondary-to-primary weight flow ratio, 0.015.

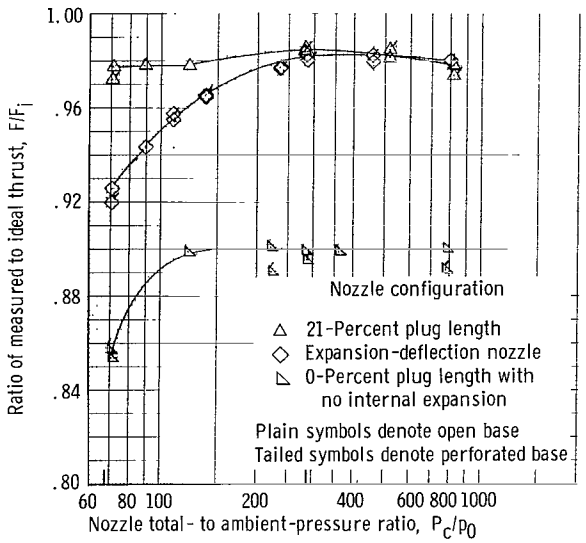

Figure 13. - Effect of bleed geometry on nozzle performance. Corrected secondary- to primary weight flow ratio, 0.015.

The effect of secondary flow passage geometry on nozzle performance is presented in figure 13. Data were obtained from figure 9 for $(W_s/W_o)\sqrt{T_s/T_p} = 0.015$. It was shown that this small amount of secondary flow increases the nozzle performance primarily through an increase in the base force. An additional increase in nozzle efficiency possibly may be achieved by increasing the momentum of the secondary flow through an increase in flow velocity. This increase was arbitrarily accomplished by restricting the secondary flow passage with a perforated base plate (see fig. 4(b)). The ratio of the perforated base flow area to the open base flow area thus obtained was 0.20. The effect of this flow geometry is shown for the 0-percent plug without internal expansion, the 21-percent plug, and the E-D nozzle. Tailed symbols denote nozzle performance for the perforated base, and plain symbols denote nozzle performance for the open base. The efficiencies of the perforated base plug nozzles were comparable with those of the open base. The efficiency of the perforated base E-D nozzle was either comparable with or slightly less than that of the open base. Thus, for this small amount of secondary flow, the geometry of the secondary flow passage did not have a significant effect on nozzle performance.

External Flow Effects

On the basis of quiescent performance, the full-length plug nozzle and the truncated plug nozzles with internal expansion appear to be the most attractive concepts of those investigated for providing altitude compensation. Therefore, these configurations were tested to determine external flow effects. Nozzle performance was obtained in the 8- by 6-foot (2.44- by 1.83-m) supersonic wind tunnel at free-stream Mach numbers of 0.56, 0.80, 1.0, 1.37, and 1.97.

Measured nozzle performance with external flow is compared with quiescent performance, as well as with calculated external flow performance. The calculation procedure utilizes measured quiescent performance, which is corrected for boattail drag, lip drag, and overexpansion losses.

Boattail drag is defined as the drag force on the boattail surface, and lip drag is defined as the drag force on the boattail base. Both drag terms were obtained by integrating the pressure forces measured at a given nozzle pressure ratio and free-stream Mach number. Overexpansion losses were determined for the nozzle "apparent" pressure ratio (i.e., the ratio of the nozzle total pressure to the lip pressure), since overexpansion results from the fact that, with external flow the nozzle expands to lip pressure rather than to ambient pressure. The following procedure was used to determine overexpansion losses: An internal thrust coefficient was calculated with the use of the quiescent thrust coefficient and the ambient drag term,

$$C_{F_{internal}} = C_{F_{quiescent}} + \left(\frac{p_0}{P_c}\right)\left(\frac{A}{A^*}\right)$$

The internal thrust coefficient was then plotted as a function of the nozzle pressure ratio. This curve, not presented herein, was entered at the nozzle apparent pressure ratio to determine the corresponding internal thrust coefficient with external flow. The corrected thrust coefficient, which now included overexpansion losses, could then be calculated from the following equation:

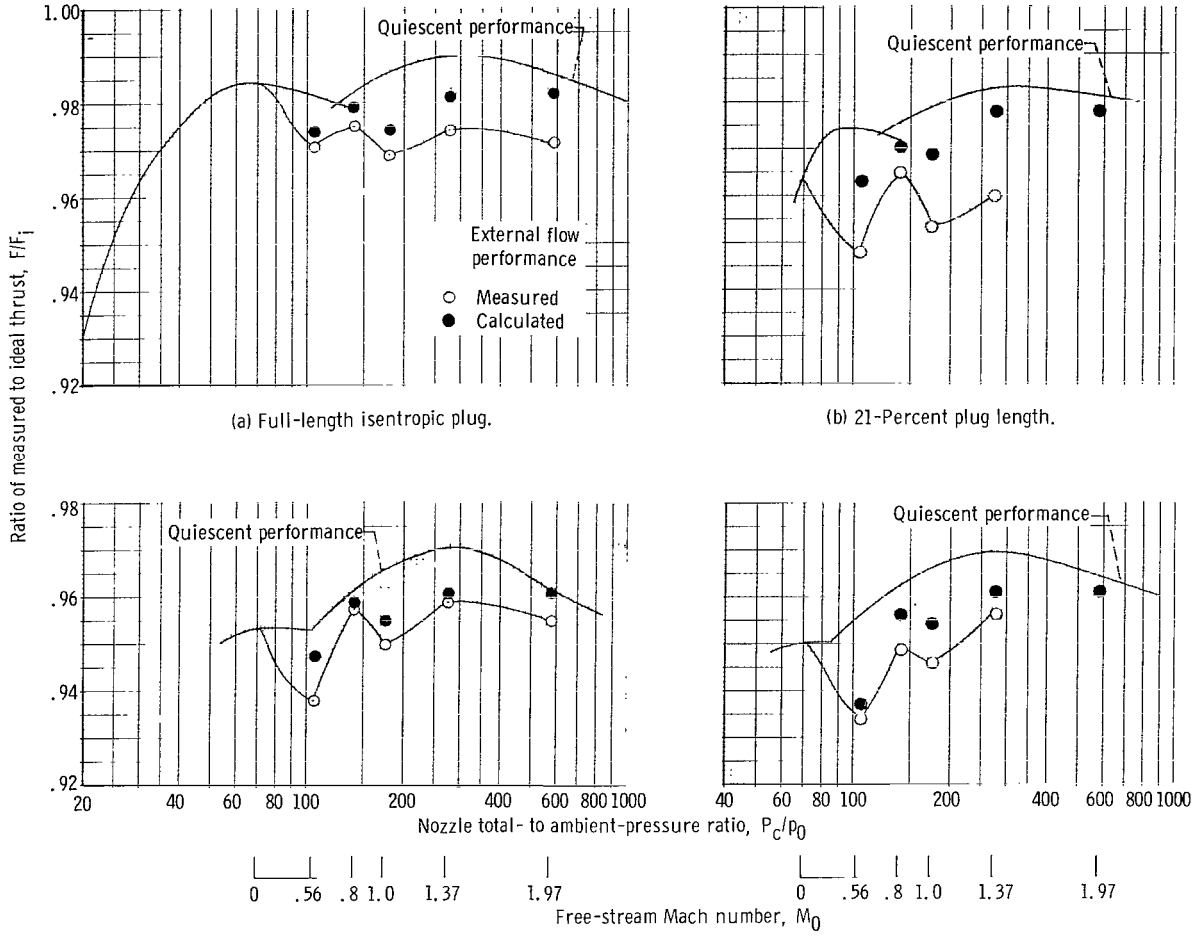

Figure 14. - External flow effects on nozzle performance without secondary flow.

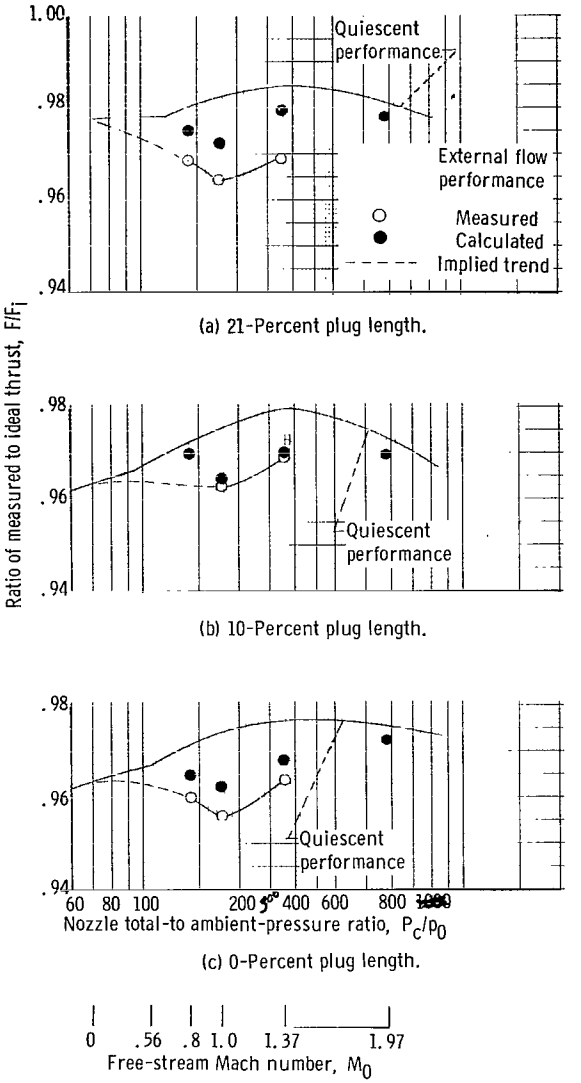

Figure 15. - External flow effects on nozzle performance with secondary flow and open base. Corrected secondary-to-primary weight flow ratio, 0.015.

$$C_{F_{corrected}} = \left(C_{F_{internal}}\right)_{\substack{\text{at apparent} \\ \text{pressure ratio}}} - \left(\frac{p_0}{P_c}\right)\left(\frac{A}{A^*}\right)$$

where p_0 was the free-stream static pressure. Finally, the nozzle efficiency with external flow was calculated from

$$\frac{F}{F_i} = \frac{C_{F_{corrected}} - C_{D_{boattail}} - C_{D_{lip}}}{C_{F_i}}$$

This nozzle efficiency is denoted by the solid symbols in figures 14 and 15, and the measured nozzle efficiencies are denoted by the open symbols.

The external flow effects on plug nozzle performance without secondary flow are shown in figure 14. Data for the full-length plug and for the 21-, 10-, and 0-percent plug lengths are presented in figures 14(a) to (d), respectively. The external flow performance was less than the quiescent performance and varied in an oscillatory manner between sea level and Mach 1.0. In a later figure, this oscillation will be shown to result from a variation in the relative significance of overexpansion losses and drag effects in this region of the trajectory. Above Mach 1.0, the external flow effects gradually decreased, and the performance approached the quiescent performance. However, it is possible that at sufficiently high altitudes the billowing jet plume, due to the underexpanded nozzle flow, could separate the flow over the boattail. Thus, the external flow performance could be greater than the quiescent performance as a result of the increase in boattail pressure force.

The calculated external flow performance generally agreed well with the measured performance. The trends in the curves were similar, and the magnitude of the nozzle efficiency generally agreed within 1 percent. The calculated performance does not include external model friction, which accounts in part for the difference between calculated and measured efficiency.

The external flow effects on nozzle performance with secondary flow are presented in figure 15. The corrected secondary-to-primary weight flow ratio was 0.015. Data for the 21-, 10-, and 0-percent plug lengths are presented in figures 15(a) to (c), respectively. The variations in performance with trajectory conditions and the comparisons of calculated and measured performance were similar to those without secondary flow. Data were not obtained at Mach 0.56; therefore, the trend in the curve for Mach numbers of less than 0.8 is implied.

In figure 16 is presented the generalized performance loss due to external flow effects, where performance loss (expressed in percent of ideal thrust) is the difference between the external flow performance and the quiescent performance. The performance loss for the case of no secondary flow is presented in figure 16(a), as obtained from figure 14. In general, the maximum loss in nozzle efficiency was approximately 2.5 percent and occurred at Mach numbers of 0.5 and 1.0. Thus, external flow effects are small and confined to a limited part of the trajectory.

The effect of secondary flow on the generalized performance loss is shown in figure 16(b) for a corrected secondary-to-primary weight flow ratio of 0.015, as obtained

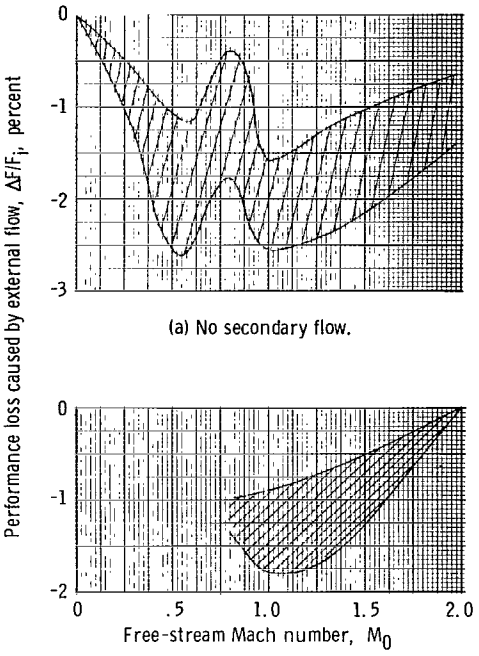

(a) No secondary flow.

(b) Corrected secondary-to-primary weight flow ratio, 0.015; open base.

Figure 16. - Generalized performance loss due to external flow effects.

from figure 15. This figure shows that secondary flow reduced the magnitude of the performance loss, in that the maximum value was reduced from 2.5 to 1.75 percent. The data band is not complete at subsonic Mach numbers, since nozzle performance was generally not obtained for Mach numbers of less than 0.8.

The variation of boattail drag, lip drag, and overexpansion loss with free-stream Mach number is presented in figure 17 and is typical of all configurations. Drags and overexpansion loss are expressed in percent of nozzle ideal thrust. The curves for boattail and lip drag exhibited a typical transonic drag rise and peaked at Mach 1.0. The maximum boattail drag was only 0.8 percent of ideal thrust, whereas the maximum lip drag was only 0.15 percent. The peak of the overexpansion loss, however, occurred at Mach 0.5 and had a value of 0.425 percent. The occurrence of peak effects at differing Mach numbers would explain the oscillations in the curves for external flow performance.

SUMMARY OF RESULTS

An experimental investigation was made of the performance of annular plug and expansion-deflection (E-D) nozzles, and included the effects of external flow at Mach

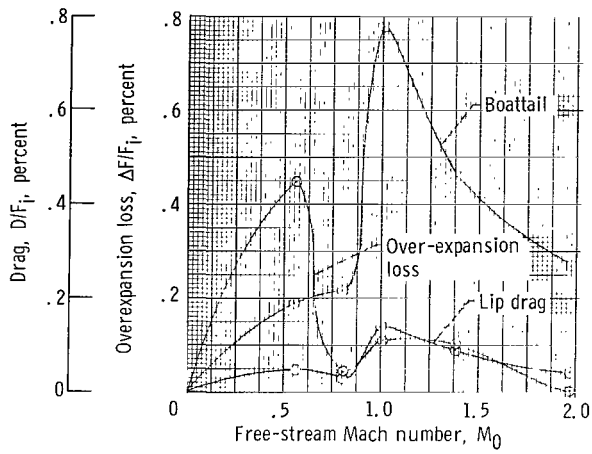

Figure 17. - Typical variation of boattail drag, lip drag, and overexpansion loss.

numbers ranging from 0.56 to 2.0. The effects of base bleed were also studied as well as geometry variations, which included plug length and nozzle internal expansion. The following results were obtained:

1. The full-length plug nozzle provided a nearly constant and optimum quiescent performance, whereas the E-D nozzle exhibited a performance only comparable with that of a 15^{o}-convergent-divergent (C-D) nozzle. Thus, the plug nozzle was altitude compensating, whereas the E-D nozzle was not. Values of plug nozzle efficiency ranged from 98.4 percent at sea level to 99 percent at the design pressure ratio of 290. Efficiencies of the E-D and C-D nozzles, respectively, were 92.3 and 92.6 percent at sea level, and 97.6 and 97.8 percent at the design point.

2. Truncation of the plug nozzles with internal expansion to 21, 10, and 0 percent of the full plug length resulted in decreased nozzle performance that varied, respectively, from 96.4, 95.3, and 94.9 percent at sea level to 98.3, 97.0, and 96.8 percent at the design point. Thus, the performance of the 21-percent-length plug nozzle was better than that of the ~~full-length plug~~ E-D nozzle, whereas the 0- and 10-percent plug nozzle performance was better than that of the C-D nozzle near sea level only.

3. Secondary flow, in corrected amounts as small as 1.5 percent of the primary flow, produced improvements at all nozzle pressure ratios in the performance of the truncated plug nozzles with internal expansion. Also, nozzle efficiencies were greater than or comparable with that of the C-D nozzle. The E-D nozzle, however, had better performance only at nozzle pressure ratios above the design value of the C-D nozzle.

4. The improvement in truncated plug nozzle performance with small amounts of secondary flow was primarily a result of increased base pressure. The tested geome-

tries of the secondary flow passage did not have a significant effect on nozzle performance for small flow rates.

5. Elimination of both the internal expansion and the external plug surface, while the same design area ratio was maintained, resulted in poor nozzle performance, even with secondary flow.

6. External flow effects were small and confined to a limited part of the trajectory. The maximum loss in performance was approximately 2.5 percent of the ideal thrust and occurred below Mach 1.0. Secondary flow reduced the performance loss to as little as 1.75 percent of ideal thrust. Substantial agreement was seen between measured plug nozzle performance and semiempirical predictions based on quiescent performance.

Lewis Research Center,
National Aeronautics and Space Administration,
Cleveland, Ohio, October 4, 1967,
128-31-11-03-22.

REFERENCES

1. Alexander, George: NASA Considers Recoverable Lifting Body Boost Vehicle. Aviation Week, vol. 80, no. 26, June 29, 1964, pp. 38-51.

2. Carlson, R. A.; Divita, J. S.; Nelson, D. A.; and Rosemary, J. K.: Advanced Aerodynamic Spike Configurations. Rep. No. R-5940-3, Rocketdyne Div., North American Aviation, Aug. 1965. (Available from DDC as AD-366526.)

3. Connors, James F.; Cubbison, Robert W.; and Mitchell, Glen A.: Annular Internal-External-Expansion Rocket Nozzles for Large Booster Applications. NASA TN D-1049, 1961.

4. Rao, G. V.R.: Approximation of Optimum Thrust Nozzle Contour. ARS J., vol. 30, no. 6, June 1960, pp. 561-563.

5. Connors, James F.; and Meyers, Rudolph C.: Design Criteria for Axisymmetric and Two-Dimensional Supersonic Inlets and Exits. NACA TN 3589, 1956.

6. Beheim, Milton A.: Flow in the Base Region of Axisymmetric and Two-Dimensional Configurations. NASA TR R-77, 1961.

7. Korst, H. H.; Page, R. H.; and Childs, M. E.: A Theory for Base Pressures in Transonic and Supersonic Flow. Tech. Note 392-2 (AFOSR TN 55-89), Eng. Exp. Station, University of Illinois, Mar. 1955.

8. Korst, H. H.; Page, R. H.; and Childs, M. E.: Compressible Two-Dimensional Jet Mixing at Constant Pressure. Tables of Auxiliary Functions for Fully Developed Mixing Profiles. Tech. Note 392-3 (AFOSR TN 55-99), Eng. Exp. Station, University of Illinois, Apr. 1955.

9. Korst, H. H.; and Chow, W. L.: Compressible Non-Isoenergetic Two-Dimensional Turbulent (Prt=1) Jet Mixing at Constant Pressure - Auxiliary Integrals, Heat Transfer and Friction Coefficients for Fully Developed Mixing Profiles. Tech. Note 392-4 (AFOSR TN 59-20), Eng. Exp. Station, University of Illinois, Jan. 1959.

10. Goethert, B. H.; and Barnes, L. T.: Some Studies of the Flow Pattern at the Base of Missiles with Rocket Exhaust Jets. Tech. Rep. 58-12 (rev.), Arnold Engineering Development Center, June 1960.

11. Baughman, L. Eugene; and Kochendorfer, Fred D.: Jet Effects on Base Pressures of Conical Afterbodies at Mach 1.91 and 3.12. NACA RM E 57E06, 1957.

"The aeronautical and space activities of the United States shall be conducted so as to contribute . . . to the expansion of human knowledge of phenomena in the atmosphere and space. The Administration shall provide for the widest practicable and appropriate dissemination of information concerning its activities and the results thereof."

—NATIONAL AERONAUTICS AND SPACE ACT OF 1958

NASA SCIENTIFIC AND TECHNICAL PUBLICATIONS

TECHNICAL REPORTS: Scientific and technical information considered important, complete, and a lasting contribution to existing knowledge.

TECHNICAL NOTES: Information less broad in scope but nevertheless of importance as a contribution to existing knowledge.

TECHNICAL MEMORANDUMS: Information receiving limited distribution because of preliminary data, security classification, or other reasons.

CONTRACTOR REPORTS: Scientific and technical information generated under a NASA contract or grant and considered an important contribution to existing knowledge.

TECHNICAL TRANSLATIONS: Information published in a foreign language considered to merit NASA distribution in English.

SPECIAL PUBLICATIONS: Information derived from or of value to NASA activities. Publications include conference proceedings, monographs, data compilations, handbooks, sourcebooks, and special bibliographies.

TECHNOLOGY UTILIZATION PUBLICATIONS: Information on technology used by NASA that may be of particular interest in commercial and other non-aerospace applications. Publications include Tech Briefs, Technology Utilization Reports and Notes, and Technology Surveys.

Details on the availability of these publications may be obtained from:

SCIENTIFIC AND TECHNICAL INFORMATION DIVISION

NATIONAL AERONAUTICS AND SPACE ADMINISTRATION

Washington, D.C. 20546